# INTERACTION OF TWO TRIBUTARY GLACIER BRANCHES AND IMPLICATIONS FOR SURGE BEHAVIOR

By

Christopher P. Knowles, B.S.

A Thesis Submitted in Partial Fulfillment of the Requirements

for the Degree of

Master of Science

in

Physics

University of Alaska Fairbanks

May 2018

APPROVED:

Martin Truffer, Committee Chair
Chris Larsen, Committee Member
David Newman, Committee Member
Renate Wackerbauer, Committee Member
Renate Wackerbauer, Chair
*Department of Physics*
Anupma Prakash, Interim Dean
*College of Natural Science and Mathematics*
Michael Castellini, *Dean of the Graduate School*

**Abstract**

A glacier surge is a dynamic phenomenon where the glacier after a long period of quiescence, increases its velocities by up to two orders of magnitude. These surges tend to have complex interactions with tributaries, yet the role of these tributary interactions towards glacier surging has yet to be fully investigated. In this work we construct a synthetic glacier with an adjustable tributary intersection angle to study tributary interaction with the trunk glacier. The geometry we choose is loosely based on the main trunk and tributary interaction of Black Rapids Glacier, AK, USA, which last surged in 1936-1937. We investigate surface elevations, medial moraine locations, and erosive power at the bed of the glacier in response to our adjustable domain and relative flux. A nonlinear relationship between tributary flux and surface elevations is found that indicates flow restrictions can occur with geometries like Black Rapids Glacier. These flow restrictions cause increased ice thicknesses up-glacier which can lead to surges via increased stresses.

## Table of Contents

## List of Figures

**Page**

**Acknowledgements**

I would like to thank my advisor Dr. Martin Truffer for his ceaseless support during my time working with him. His encouragement and guidance was paramount in my completion of this work and my growth as a researcher. My committee members Dr. Chris Larsen, Dr. David Newman, and Dr. Renate Wackerbauer greatly improved the quality of my writing and I will always be thankful for the time they spent to help me through my years here at UAF. This work would not have been possible without the work previously done by Douglas Brinkerhoff whose finite element model was the basis for the work I present.

My accomplishments and passions in life are thanks to my parents and their emphasis on academics has always motivated me to pursue my education in physics. I've been able to enjoy so much of Alaska due to the adventures Mariah and her family would take me on and I can never thank them or my parents enough for the support and love they have shown me.

I would like to acknowledge partial support from NSF Polar Programs grants OPP-1107491 and OPP 1304899. I would also like to acknowledge partial support from the UAF Physics department for providing me with the opportunity to work as a teaching assistant during my time working towards my degree.

# Chapter 1
# Introduction

A glacier in its simplest form is a body of ice that deforms due to its own weight. This driving stress leads to ice flow through deformation and sliding that transports ice from an accumulation area to an ablation area. The accumulation of ice occurs through snowfall at higher elevations, adding mass to the glacier which is later lost as meltwater or icebergs at lower elevations (Cuffey and Paterson, 2010). For the glacier to be in balance the mass gain and mass loss terms are equal and compensated by ice flow. Where the glacier accumulates snow it loses mass through flow and where ice melts the glacier adds mass through flow. In a certain class of glacier, known as surge-type glaciers, the surface is in a constant dynamic adjustment because that balance is not maintained as the phases of flow are either too large or too small. Even non-surge-type glaciers that are retreating are approximately in balance when compared to the extreme imbalance that occurs for surge-type glaciers. The flow instabilities found in surge-type glaciers make for a rich area of study for glacier dynamics.

## 1.1 Glacier Surges

A glacier surge is defined by a multiyear, quasi-periodic oscillation between extended periods of normal motion and brief periods of comparatively fast motion (Raymond, 1987). These quasi-periodic changes in glacier flow are known as the glacier's quiescent and surge phases. In regions with temperate glaciers (ice at melting point) such as Alaska, there are relatively rapid surge cycles where the active phase is short and intense (several months to a few years), compared to regions with polythermal glaciers (comprised of warm and cold ice), such as Svalbard, where the surge phase is more long-lived (~10 years) (Copland and others, 2003). During the quiescent phase glacier flow is too low for the glacier to be in a steady state with the climate. Thus, during this phase, ice builds up in a reservoir area and is lost in a receiving area. These areas do not always coincide with the accumulation area or the ablation area. This returns the glacier to near its pre-surge state (Raymond, 1987). The duration of quiescence is not uniform. Polythermal glaciers in Svalbard have quiescent phases of 50-100 years, while temperate glaciers like those found in coastal Alaska have quiescent phases of 20-30 years (Meier and Post, 1969). During a surge phase the glacier can experience flow that is 10-1000 times faster than in quiescence. Ice stored in the upper

reservoir zone is transferred down-glacier during the surge to a receiving zone, and the terminus of the glacier can advance several kilometers (Murray and others, 2003). These surges can pose a natural hazard by overrunning infrastructure or damming lakes and rivers that can later cause flooding when the glacier retreats (Kargel and others, 2005). While surges are widely accepted to be in response to internally driven oscillations in basal conditions (Sevestre and Benn, 2015), there is still uncertainty in surge mechanisms since characteristics of surge-type glaciers can vary greatly.

The surge phenomenon is recognized as one of the outstanding unsolved problems of glacier mechanics (Kamb and others, 1985). Studies which try to quantify surging glaciers under varied mechanisms such as Murray and others (2003), Hamilton and Dowdeswell (1996), Raymond (1987), Jiskoot and others (2017), King and others (2015), and Sevestre and Benn (2015) have not been able to identify a surge mechanism that explains all mechanisms presented under a unified theory. To date, Sevestre and Benn (2015) presented the most promising effort through an enthalpy model attempting to unify thermal and hydraulic switch mechanisms. In this model the optimal surge zone occurs where neither heat conduction nor runoff can effectively discharge heat gains. These heat gains occur as gravitational potential energy and is converted into warming or melting ice. The surge zone then depends on the climate the glacier experiences, the bed materials, the drainage system type, and other factors.

The changing climate can create a new set of surging glaciers that has not been observed in years past. Hewitt (2007) suggests that the progressive warming of ice over the past century has the potential to trigger a surge in glaciers that are currently not showing symptoms of surging. There is a temporal clustering of surge events where, for example, 10 surge-type tributaries formerly out-of-phase by decades in the Himalayas had a convergence of surge events (Hewitt, 2007). Eisen and others (2005) found that local changes in the average mass balance changed the duration of surge cycles. An early termination of an active surge at Variegated Glacier in 1995 caused the surge front to remain located in the middle part of the glacier. This termination seems to have influenced the length of recovery time needed to re-initiate an active surge on Variegated Glacier (Eisen and others, 2005). Conversely some surge-type glaciers in the past have switched to becoming non-surge type. Kienholz and others (2017) found that even with current climate scenarios (and for projected climate

scenarios) that Black Rapids Glacier is not likely to surge due to mass starvation and a lack of thickening in the reservoir area.

### 1.2 Characteristics of a Surging Glacier

To identify a surge-type glacier from an observational standpoint Meier and Post (1969) lay out a list of criteria to be met, such as looped moraines, heavy surface crevassing, and pushed moraines. There is a non-random distribution where some glacierized areas have surging glaciers (Southeast Alaska, Svalbard, Iceland, Greenland) and others do not (European Alps, New Zealand, mainland Scandinavia) (Raymond, 1987). There is a high association of surging glaciers in the Alaska Range on the Denali fault, however other major fault zones with active tectonism do not contain surging glaciers (Meier and Post, 1969; Harrison and Post, 2003). Attempts to quantify this distribution shows that surging is probably a product of more than one environmental condition (Hamilton and Dowdeswell, 1996). Global catalogs of surge-type glaciers have found that surges occur in all manner of glaciers such as land terminating and tidewater, cirque, along with valley glaciers or ice streams (Murray and others, 2003). Sevestre and Benn (2015) give further characteristics by comparing between surge and non-surge glaciers that coexist. Surge-type glaciers tend to be longer, exist at higher elevations, have larger areas, and have shallower surface slopes. There are no clear geological or climatological identifiers that can be used to classify all types of surge-type glaciers.

### 1.3 Surge Initiation

The mechanisms behind surge initiation are not well understood, but there is some consensus that a critical geometry in terms of slope and ice thickness needs to be reached in order to alter the basal shear stress (Raymond, 1987). Glaciers are found on either hard bedrock or soft sediment/till, sometimes a mixture of both. Harrison and Post (2003) speculated that the controlling effect might be permeability of the underlying rock because of the association of surging on faults mentioned previously. Surging disrupts the hydraulic system which would lead to low basal shear stress and rapid basal motion. The disruption of the hydraulic system inducing a surge has been laid out in Raymond (1987) in which trapped englacial water can be redistributed onto the glacier bed. Surges on soft beds could be at-

tributed to till deformation and is a preferred mechanisms due to the till's highly nonlinear rheology (Harrison and Post, 2003).

### 1.3.1 Tributary Interaction

Tributaries are used to visually identify the surge history of a glacier from the looped moraines that form in response to an active surge phase such as those seen at Black Rapids Glacier (now covered by a landslide) in Fig. (1.1) and the nearby Susitna Glacier (Clarke, 1991) in Fig. (1.2). The looped moraines on Black Rapids Glacier form by the non-surge type flow from the Loket tributary during quiescence that pushes the moraine out that the surge then cuts off and displaces down glacier. The Susitna Glacier has three tributaries that all participate differently during a surge in the trunk, and also had different flow during the quiescent phase. A map showing the moraine locations before and after the 1952 surge is shown in Fig. (1.2). The northwest tributary has a large amount of flux during quiescence but almost no participation during the surge. The northeast tributary has a large amount of flux during quiescence and participated in the surge. The east tributary has near-stagnant flow during quiescence, yet had the largest participation during the surge (Clarke, 1991). Surging in a tributary has caused a surge in the trunk and vice versa as seen in the Himalayas (Hewitt, 2007). The more dendritic glaciers appear to have increased susceptibility to surging (Sevestre and Benn, 2015). They hypothesize that this is due to the branch's influence on flow restrictions, but tributary interactions have not explicitly been linked to surge initiation.

### 1.3.2 Flow Restricitons

Flow restrictions can occur along a glacier from mechanisms such as the valley curvature, bed rock undulation, a frozen bed, and tributary interaction (Jiskoot and others, 2017). Restrictive flow from a confluence zone can result in longitudinally compressive flow which allows ice mass to accumulate up-glacier of the confluence (King and others, 2015; Jiskoot and others, 2017; Clarke, 1991).

Flow restrictions in the trunk glacier tend to occur when the tributary/trunk junction is at a near-right-angle and when the cross-sectional area of the tributary and trunk are similar

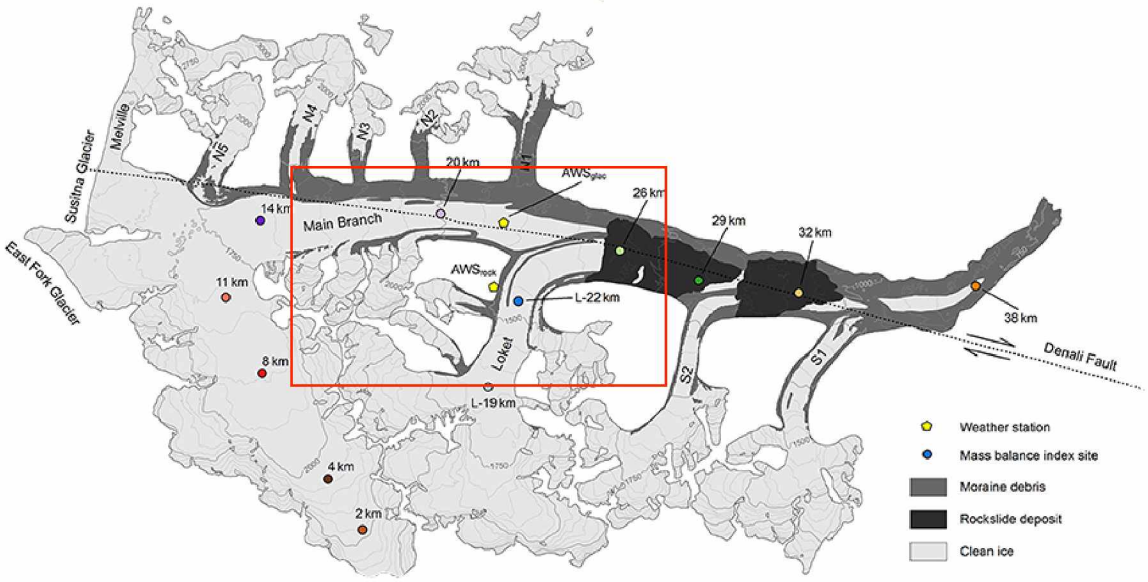


Figure 1.1. *Map of Black Rapids Glacier showing orientation of the Loket tribuary with the main branch. The Denali Fault is traced as a dashed curve. The geometry within the red box containing the main flow and the Loket tributary is the domain we base our synthetic glacier on. The distance labels are measured along an approximate flowline from the highest surface elevation of the glacier. Modified from Kienholz and others (2017).*

(Jiskoot and others, 2017). Potential flow restrictions due to tributary interaction have been observed at Black Rapids Glacier (see Fig. (1.1)). Dynamic ice thickening through this flow restriction at Black Rapids created by the Loket tributary had caused ice thickness changes up-glacier of the confluence of ~50 m between 1949 and 1977 (Heinrichs and others, 1996; Shugar and others, 2010). Observations of flow for more acute angles show that flow should be faster in the confluence and aligned with the trunk glacier's flow (Gudmundsson, 1999; Satyabala, 2016).

The effects of a tributary on a trunk glacier with respect to the angle of the tributary's entrance have not been studied in relation to surge susceptibility. Other work with respect to tributary flow modeling has been done by Gudmundsson (1999) through 3-D finite element methods by varying flow parameters and then inspecting vertical velocity profiles, medial moraine construction, and vertical strain rates near the confluence junction. Oerlemans and van Pelt (2015) modeled the Abrahamsenbreen glacier which has 10 tributaries

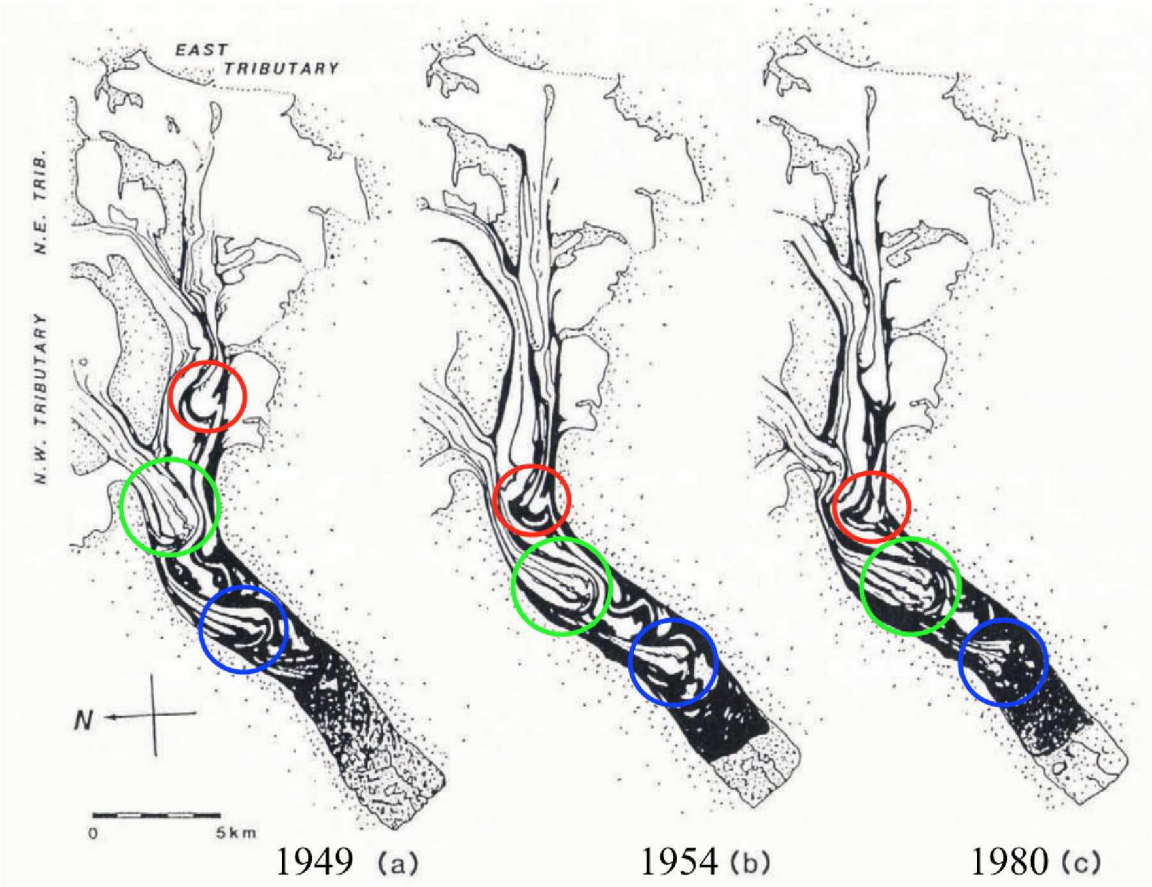


Figure 1.2. *Map of Susitna Glacier's tributaries. Three distinct moraines can be monitored and are circled in red, green, and blue. Note that the green moraine did not extend as far as the blue did from a surge before the 1952 surge. (a) corresponds to before the surge, (b) is after the surge, and (c) is 26 years after the 1951-52 surge. Modified from Clarke (1991).*

flowing into a main trunk, where most appear to be intersecting at a near right angle. They define ice thickness with a surge parameter which, when altered, will mimic the effects a surge would have on the glacier's thickness. Since their surges were imposed instead of internally generated they could only inspect the response a glacier would have to a surge event.

## 1.4 Objectives

This work was motivated by the surge at Black Rapids Glacier in 1936 in which the Loket Tributary contributed to a surge that extended the terminus roughly 6.5 km into the Delta River valley. The result of Heinrichs and others (1996) indicate that the main branch of the glacier was being dammed by steady flow into the main branch from the Loket tributary, resulting in thickening above the tributary entrance.

In this work we construct a synthetic glacier with an adjustable tributary intersection angle to study tributary interaction with the trunk glacier. The geometry we choose is loosely based on Black Rapids Glacier's main trunk and the Loket tributary. The goal of this work is to inspect the impact of changing tributary conditions such as its angle of intersection and amount of ice that flows from it. This will be of use for improving the current understanding of what factors are relevant towards surge initiation.

# Chapter 2
# Model Setup

## 2.1 Field Equations

Considering a Cartesian coordinate system (x,y,z) with the z axis pointing vertically upward (z=0 at sea level), the conservation of mass for an incompressible fluid and conservation of momentum can be written as

$$\nabla \cdot \mathbf{u} = 0 \tag{2.1}$$

$$\rho \frac{d\mathbf{u}}{dt} = \nabla \cdot \sigma + \rho \mathbf{g} = 0 \tag{2.2}$$

where $\mathbf{u}$ is the 3-D velocity field, $\rho$ is the ice density, $\mathbf{g}$ is gravitational acceleration, and $\sigma$ is the Cauchy stress tensor (Cuffey and Paterson, 2010). The inertial term on the LHS of Eq.(2.2) will be neglected, which leads to the equation of incompressible Stokes flow.

The constitutive equation governing the steady-state creep in ice and relating deviatoric stresses $\sigma'_{ij}$ to strain rates $\dot{\epsilon}_{ij}$ is expressed as (Cuffey and Paterson, 2010)

$$\sigma'_{ij} = 2\eta \dot{\epsilon}_{ij}, \quad \eta = \frac{1}{2} A^{-\frac{1}{n}} \dot{\epsilon}^{\frac{(1-n)}{2n}} \tag{2.3}$$

where $\dot{\epsilon}^2 = \frac{1}{2}\dot{\epsilon}_{ij}\dot{\epsilon}_{ij}$ is the second invariant of the strain-rate tensor and repeat indices imply summation. Deviatoric stresses are defined in terms of stress components, $\sigma'_{ij} = \sigma_{ij} - \frac{1}{3}\sigma_{ii}\delta_{ij}$, where $\delta_{ij}$ is the Kronecker delta function. Results from experiments point towards $n = 3$ (Cuffey and Paterson, 2010), and the flow rate factor $A = 3.4 \times 10^{-24}$ Pa$^{-3}$ s$^{-1}$ used for temperate glaciers was found to best fit observations at Black Rapids Glacier (Truffer and others, 2001).

Eq.(2.2) can be vertically integrated to define the horizontal stress field equations (Pattyn, 2002).

$$2\frac{\partial \sigma'_{xx}}{\partial x} + \frac{\partial \sigma'_{yy}}{\partial x} + \frac{\partial^2}{\partial x^2}\int_z^S \sigma'_{xz} dz - \tau_{bx} = \rho g \frac{\partial (S)}{\partial x} \tag{2.4}$$

$$2\frac{\partial \sigma'_{yy}}{\partial y} + \frac{\partial \sigma'_{xx}}{\partial y} + \frac{\partial^2}{\partial y^2}\int_z^S \sigma'_{yz} dz - \tau_{by} = \rho g \frac{\partial (S)}{\partial y} \tag{2.5}$$

where $\tau_{bx}$ and $\tau_{by}$ are components of the basal shear stress in the x and y direction and S is the surface of the glacier. Note that we assume that pressures are hydrostatic and that

stresses related to horizontal gradients of vertical velocities are negligible (Brinkerhoff and Johnson, 2015). This vertical integration takes into account boundary conditions at the base and surface of the glacier. At the surface we have a stress-free condition, while at the bottom the basal drag $\tau_b$ and a basal velocity $\mathbf{u_b}$ are related through a friction coefficient $\beta^2$ by

$$\boldsymbol{\tau}_b = \mathbf{u_b}\beta^2 \tag{2.6}$$

where the friction coefficient is a positive scalar quantity (Pattyn and others, 2008). After this vertical integration, our 3-D space now becomes a 2-D plane (map plane) in (x,y).

With the relation for the strain-rate tensor to velocity gradients given as

$$\dot{\epsilon}_{ij} = \frac{1}{2}\left(\frac{\partial u_i}{\partial x_j} + \frac{\partial u_j}{\partial x_i}\right) \tag{2.7}$$

we can combine the horizontal stress field equations (2.4),(2.5) and the flow law equation (2.3) (Pattyn, 2002).

Through vertically integrating the mass balance equation and using kinematic boundary conditions at the surface of the glacier we obtain an expression for the change of local ice thickness

$$\frac{\partial H}{\partial t} = -\nabla \cdot (H\bar{\mathbf{u}}) + \dot{a} \tag{2.8}$$

where H is the ice thickness (m), $\bar{\mathbf{u}}$ is the depth-averaged horizontal velocity vector (m $a^{-1}$), and $\dot{a}$ is the surface mass balance (m $a^{-1}$ ice equivalent).

## 2.2 Finite Element Method

The Finite Element Method (FEM) is a method that converts the field equations into a discrete variational form that can then be numerically solved. To define the variational problem we will be following methods presented in Brinkerhoff and Johnson (2015).

### 2.2.1 Weak Form

We define the weak form of Eq. (2.4), (2.5) (the Blatter-Pattyn equations) by first adopting the $\xi$ coordinate

$$\xi = \frac{S - z}{H}$$

that changes the vertical domain to go from 0 at the surface to 1 at the bed. Multiplying the conservation of momentum equation with a test function $\Pi \in V$ and integrating by parts, we obtain the weak form, which is then solved for $\mathbf{u} \in \mathrm{U}$:

$$\underbrace{\int_{\bar{\Omega}} \int_1^0 [\bar{\nabla}\Pi + \frac{\partial}{\partial \xi}\Pi \nabla \xi] \cdot 2\eta \dot{\epsilon}_{ij} H d\xi d\bar{\Omega}}_{\text{Membrane and Shear Stresses}} + \underbrace{\int_{\bar{\Omega}} [\Pi \cdot \boldsymbol{\tau}_b] d\bar{\Omega}}_{\text{Basal Drag}} - \underbrace{\int_{\bar{\Omega}} \int_1^0 \Pi \cdot \rho g H \nabla S d\xi d\bar{\Omega}}_{\text{Driving Stress}} = 0 \quad (2.9)$$

where U=V=$H^1(\Omega)^2$ is the appropriate Sobolev space, $\bar{\nabla}$ is the gradient operator restricted to the horizontal domain, and $\bar{\Omega}$ is the projection of $\Omega$ (our mesh domain) onto the horizontal plane. This weak form involves the membrane and shear stresses which are balanced by the basal and driving stress.

### 2.2.2 Discretization

To discretize Eq. (2.9) we use two distinct orthogonal basis sets for the horizontal and vertical dimensions. For the vertical basis functions $\phi_0$ and $\phi_1$ the Galerkin approximation leads to an ansatz solution (2.10) for the horizontal velocity which is a combination of solutions for the shallow-ice and shallow-shelf models

$$u(\xi) = u_0 + \frac{u_1}{p}[(p+1)\xi^p - 1] \quad (2.10)$$

where $u_0$ is the depth-averaged velocity, $u_0 + u_1$ is the basal velocity, $u_0 - \frac{u_1}{p}$ is the surface velocity, and p is the polynomial degree of the trial solution which is taken to be $p = 4$.

For the horizontal basis function we use the linear Lagrange finite elements $\psi$. These can be combined to give the test function

$$\Pi^h(x, y, \xi) = \sum_{i=1}^{M} \Pi^h(x_i, y_i, 0)\psi_i(x, y)(\phi_0 + \phi_1(\xi)) \quad (2.11)$$

which is an element of the test space $V^h = U^h$. M is the number of horizontal grid locations.

Our goal is to find the function $\mathbf{u}^h \in U^h$ that will satisfy

$$\underbrace{\int_{\bar{\Omega}} \int_1^0 [\bar{\nabla}\Pi^h + \frac{\partial}{\partial \xi}\Pi^h \nabla \xi] \cdot 2\eta \dot{\epsilon}_{ij}^h H d\xi d\bar{\Omega}}_{\text{Membrane and Shear stresses}} + \underbrace{\int_{\bar{\Omega}} [\Pi^h \cdot \boldsymbol{\tau}_b] d\bar{\Omega}}_{\text{Basal Drag}} - \underbrace{\int_{\bar{\Omega}} \int_1^0 \Pi^h \cdot \rho g H \nabla S d\xi d\bar{\Omega}}_{\text{Driving Stress}} = 0 \tag{2.12}$$

Note that this equation has not been numerically integrated in the vertical direction yet. The numerical integration used in the vertical dimension uses a fourth-order Gauss-Legendre quadrature rule. After the vertical integration the equation can be solved using finite elements on the map domain $\bar{\Omega}$.

We use the Streamline Upwind Petrov-Galerkin (SUPG) stabilization method to deal with the fact that Eq. (2.8) is hyperbolic. Once we have rewritten Eq. (2.8) using SUPG we can append it to our discretized equation (Brinkerhoff and Johnson, 2015). The nonlinear variational solver is applied to a triangular mesh with roughly 14,000 to 25,000 elements depending on glacier domain. The solver comes from the FEniCS library and uses a Newton-Raphson method (Logg and others, 2012; Brinkerhoff and Johnson, 2014).

### 2.3 Glacier Geometry

The idealized geometry that we will be constructing will loosely resemble Black Rapids Glacier's confluence with the Loket tributary and is displayed in 3-D in Fig. (2.1). To construct this synthetic glacier in a mathematically adaptive form we first define the glacier bed of the tributary and trunk as inclined channels with parabolic cross section in the 3-D modeling software Google SketchUp. The tributary channel originates from the center of the main flow and pivots about that point. The angle of intersection $\theta$ between the tributary and the trunk is explicitly defined by its rotation about the pivot point, such that at $\theta = 0°$ the flows are intersecting orthogonally at the confluence zone, which is most similar to Black Rapids Glacier's geometry. Geometries in increments of 15° from $\theta = 0°$ up to $\theta = 60°$ were created to analyze effects the tributary angle has on the main glacier.

A line of intersection that changes with $\theta$ is visible when viewing the glacier bed in 3-D as seen in Fig. (2.1) and is a natural boundary to define the tributary and trunk bed separately. Using the (x,y) coordinates of our mesh where the origin $O$ is located at the

middle of the confluence the equation of these lines of intersection are defined as

$$y = \mp \tan(\frac{\pi}{4} \pm \frac{\theta}{2})x$$

where $\theta$ is the angle of intersection (60° for Fig. (2.1)) and converted to radians ($\frac{\pi}{3}$). By defining these lines of intersections as a boundary separating the two channels we avoid cases where certain (x,y) coordinates at the confluence would have two competing values of bed depth.

The main branch length is 24 km and 2 km wide, while the tributary is 12 km long and 2 km wide. This glacier domain was chosen to be sufficiently long so that unrealistic boundary conditions are dynamically removed from the area of interest at the confluence.

### 2.3.1 Meshing

We are using the open-source software GMSH which takes a given outline and creates a triangular finite element mesh within the outline with a chosen finite element density. When meshing on the domain we enforce an attractor field which increases the element density near the junction points as seen in Fig. (2.2) (Geuzaine and Remacle, 2009). Having an attractor at the junctions of the glacier is important for the solver as it is a region of high gradients in solutions and no features of the solutions can be present that are smaller than the mesh size. We create an unstructured mesh that is refined in areas with sharp edges and lower refinement where the flow is not a region of interest for computational efficiency.

## 2.4 Boundary Conditions

We enforce a no-slip condition along the lateral boundary of the glacier (u = v = 0). A minimum ice thickness (H=10m) is applied to the domain for numerical stability purposes.

## 2.5 Initial Conditions and Steady State

The accumulation and ablation terms (the mass balance function $\dot{a}$) in Eq.(2.8) are defined as zero and increase linearly when outside of our domain of interest to a maximum value at the head of the tributary and trunk as seen in Fig. (2.3). The reservoir zone has enhanced accumulation to generate ice flux as it is a numerically convenient way to supply sufficient

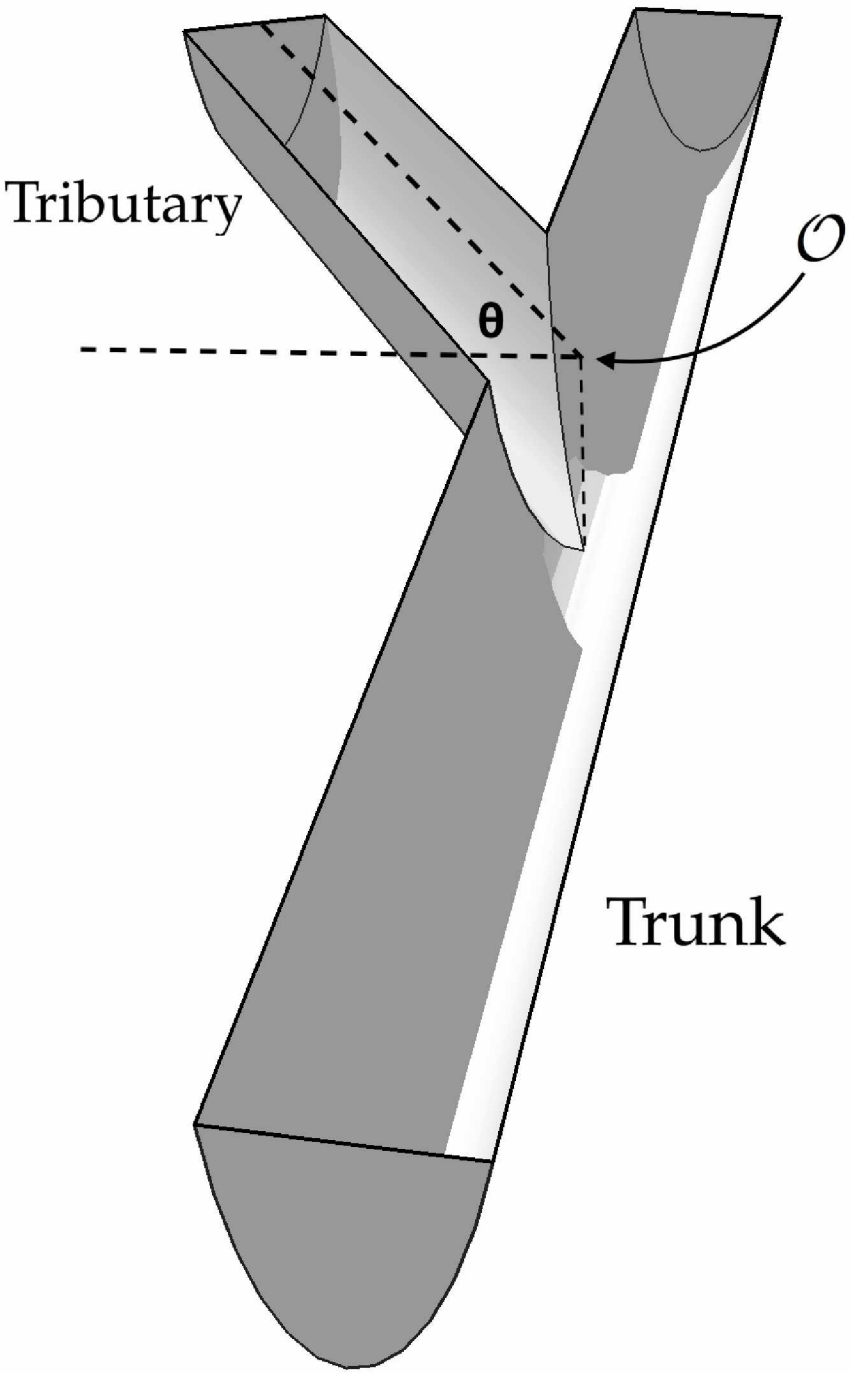


Figure 2.1. *3-D visualization of confluence zone for 60° tributary angle. The origin O is located at the pivot point between the branches, which will be the same location for all angles.*

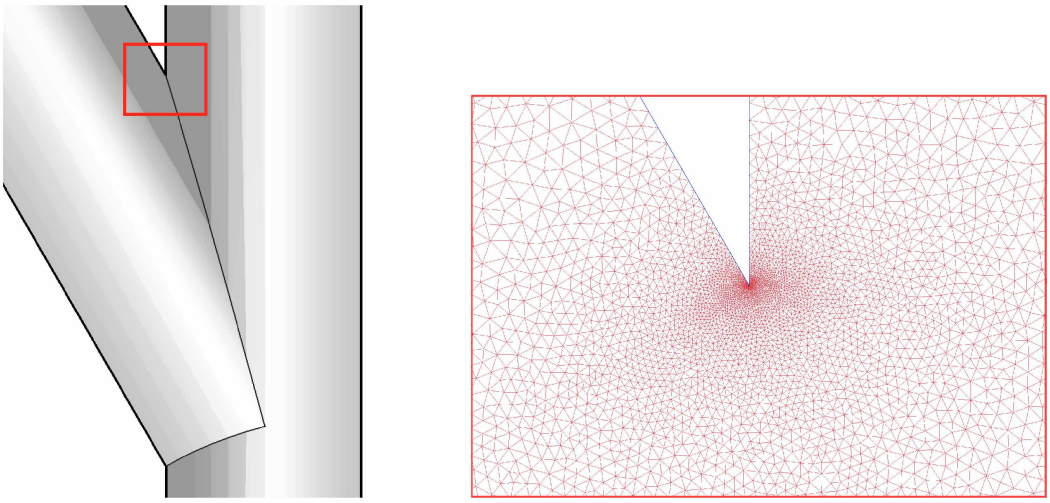

Figure 2.2. *Refined mesh at top junction of the confluence zone. The red box outlines the area of the mesh, detailed on the right.*

amounts of ice to the domain of interest without needing to expand the full model domain. The glacier branch that is outside the domain of interest but not within the reservoir zones is used as a transition zone from the unrealistic boundary conditions up-glacier in the tributary and trunk to our domain of interest (Truffer and others, 2009). The $\dot{a}$ is constant in time and is not dependent on elevation, which lets us precisely define how much ice is being accumulated and how much flux each domain produces. The mass balance function was given a value of zero in the confluence so that the tributary/trunk interaction would be based on the flux of ice into the zone and that this flux would be constant in time. The flux of the Loket tributary, main flow, and the relative flux between the two is found with

$$Q_{Main} = \int_{A_{Main}} \dot{a}(x, y) \; dA \tag{2.13}$$

$$Q_{Lok} = \int_{A_{Lok}} \dot{a}(x, y) \; dA \tag{2.14}$$

$$Q_{rel} = \frac{Q_{Lok}}{Q_{Main}} \tag{2.15}$$

where $A_{Main}$ is the area of the main flow and $A_{Lok}$ is the area of the tributary with non-zero $\dot{a}$ values as shown in Fig. (2.3). We perform several runs with the same $Q_{Main}$ and different $Q_{Lok}$ values to achieve different relative fluxes ($Q_{tributary}/Q_{Trunk}$).

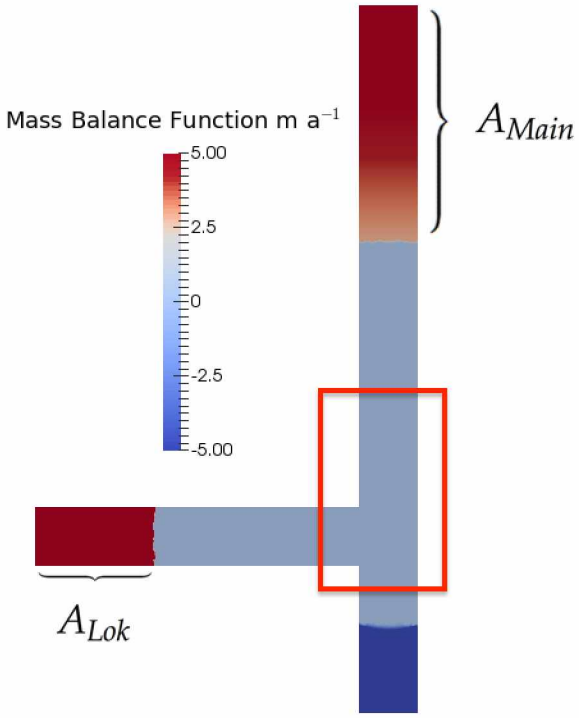


Figure 2.3. *The mass balance function $\dot{a}$ across the glacier. The domain of interest for this work is within the red box where the mass balance function is zero. Maximum values of $\dot{a}$ reach 24 m $a^{-1}$ in the tributary and 6.7 m $a^{-1}$ in the trunk, but the color scale is saturated for better visibility.*

The initial surface of the glacier is defined as a plane over the entire domain of the mesh for ease of matching boundaries of the tributary and trunk surface. With our parabolic bed and linear surface, we can take the difference of the two to obtain the initial ice thickness that the flow model will evolve to a steady state. With the understanding that the mathematical definitions of the geometries creates unphysical initial condition, we ensure the glacier has evolved to a steady state flow before evaluating fluxes. The steady state is assumed to be reached when the surface elevation does not change in time in the domain of interest.

There is some uncertainty associated with the flux continuity which could be attributed to two factors. First, the mesh size can be an issue since the total flux is obtained by integrating the flux across the glacier. The denser the mesh is the smoother the curve will

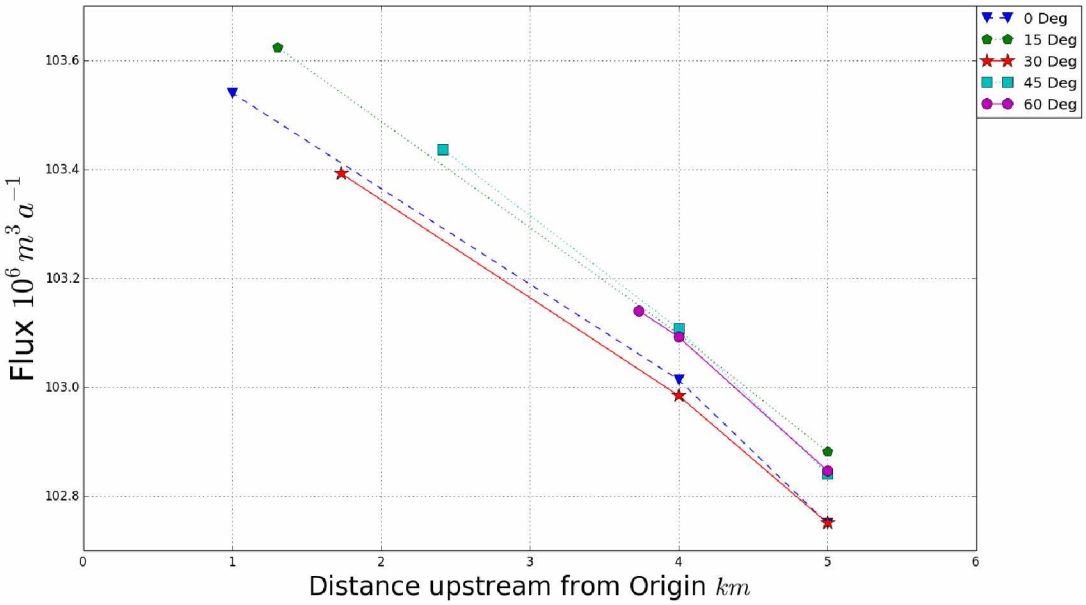


Figure 2.4. *Flux profiles across glacier taken at the position of the confluence junction, 4km, and 5km upstream of the pivot point O (Fig. (2.1)). The location of the junction changes with angle. Note that the spread in our values is small when compared to the total ice flux.*

be that we preform the trapezoidal integration on. Regions with coarser meshing will have reduced resolution which implies that the flux curve will have larger subintervals and thus a worse approximation for the flux. The second factor has to do with the enforced 10 m ice thickness that the model requires for stability. This enforced thickness creates a persistent ice flux from the boundary of the glacier walls. This flux points inward towards the centerline of the glacier from both sides. The observed increase in flux shown in Fig. (2.4) show that, as we move down-glacier towards the confluence, we are gaining an amount of ice mass which can be attributed to this enforcement of a minimal ice thickness.

We take the range of ice flux at 5 km upstream of the confluence to denote the error we can expect because for all values of $\theta$ the flux only depends on accumulation which is constant for all runs for the trunk. As we can see from observing flux at different points of the glacier, Fig. (2.4) shows that our absolute uncertainty will be $\pm 0.075 \times 10^6 m^3 a^{-1}$ where the relative uncertainty for the main flow is $\sim .07\%$ of the total flux.

# Chapter 3

# Results

We will now look at our results in terms of surface elevation, the evolution of medial moraines, and the erosive power available at the glacier bed as a function of tributary angle and tributary flux. We use the open-source data analysis and visualization application ParaView to help further visualize our results through generating streamlines, contours, and flux profiles (Ayachit, 2015).

## 3.1 Surface Elevation

### 3.1.1 Surface at and above Confluence Zone with Varied Tributary Angle

Contours shown in Fig. (3.1) show the general surface topography at steady state for the glacier. The surface contours at the confluence reflect the intersection of the trunk and tributary beds. The more orthogonal the glacier channels are the stronger the gradient of surface elevation is directly under the tributary entrance to the confluence.

We present results at 5 km upstream of the confluence center $O$ (Fig. (2.1)). Surface elevation differences at 5 km above the confluence between each angle (Fig. (3.2)) are within 2 m of each other, but are ordered in such a way that the orthogonal flow ($\theta = 0°$) had the lowest elevation and the more parallel flow ($\theta = 60°$) had the highest.

### 3.1.2 Surface above Confluence Zone with Varied Tributary Flux

We present three different scenarios for constant trunk flux and differing tributary flux with a relative flux of 0.77, 1.50, and 2.22. In Fig. (3.2) we find that the trunk surface responds to changes in tributary flux, with larger relative fluxes implying a higher surface elevation at the 5 km mark above the confluence center $O$. Since the relative fluxes roughly double each time, the trunk's surface up-glacier responds nonlinearly to change in tributary flux.

For a given relative flux there is variation in the trunk's up-glacier surface for each angle of tributary flow which increases as the relative flux increases. For a relative flux of 2.22 the surface at 5 km upstream of the confluence increases by 10 m, as the tributary angle is increased from 0° to 60°.

### 3.2 Medial Moraines Location

Location of the medial moraine is inferred by the convergence of flow lines from the trunk and tributary. As the relative flux increases so does the amount that the tributary pushes into the trunk flow. Fig. (3.3) shows the medial moraine locations for all angles and for the three cases of relative flux. Blue flow lines branching up the tributary and trunk are showing the seeding of the ice that will flow into the medial moraine. Altering the angle at which the tributary enters the trunk results in the same medial moraine after the confluence. The percentage of the total 2 km width of the trunk that the medial moraine pushes out into the confluence is 48% for 0.77, 57% for 1.5, and 63% for 2.22.

### 3.3 Erosive Power

We illustrate erosive power by calculating

$$P = \boldsymbol{\tau}_b \cdot \mathbf{u}_b = \beta^2 u_b^2 \tag{3.1}$$

for varied relative fluxes and angles (Herman and others, 2015). Fig. (3.4) generally shows relatively higher erosive power at the confluence of our synthetic glacier. At the confluence there will be an increased amount of energy available for temperate glaciers at the bed that typically will manifest as melt or erosion. More specifically Fig. (3.4) shows an increased amount of erosive power with an increased relative flux and an increase in affected glacier bed area with changing angle.

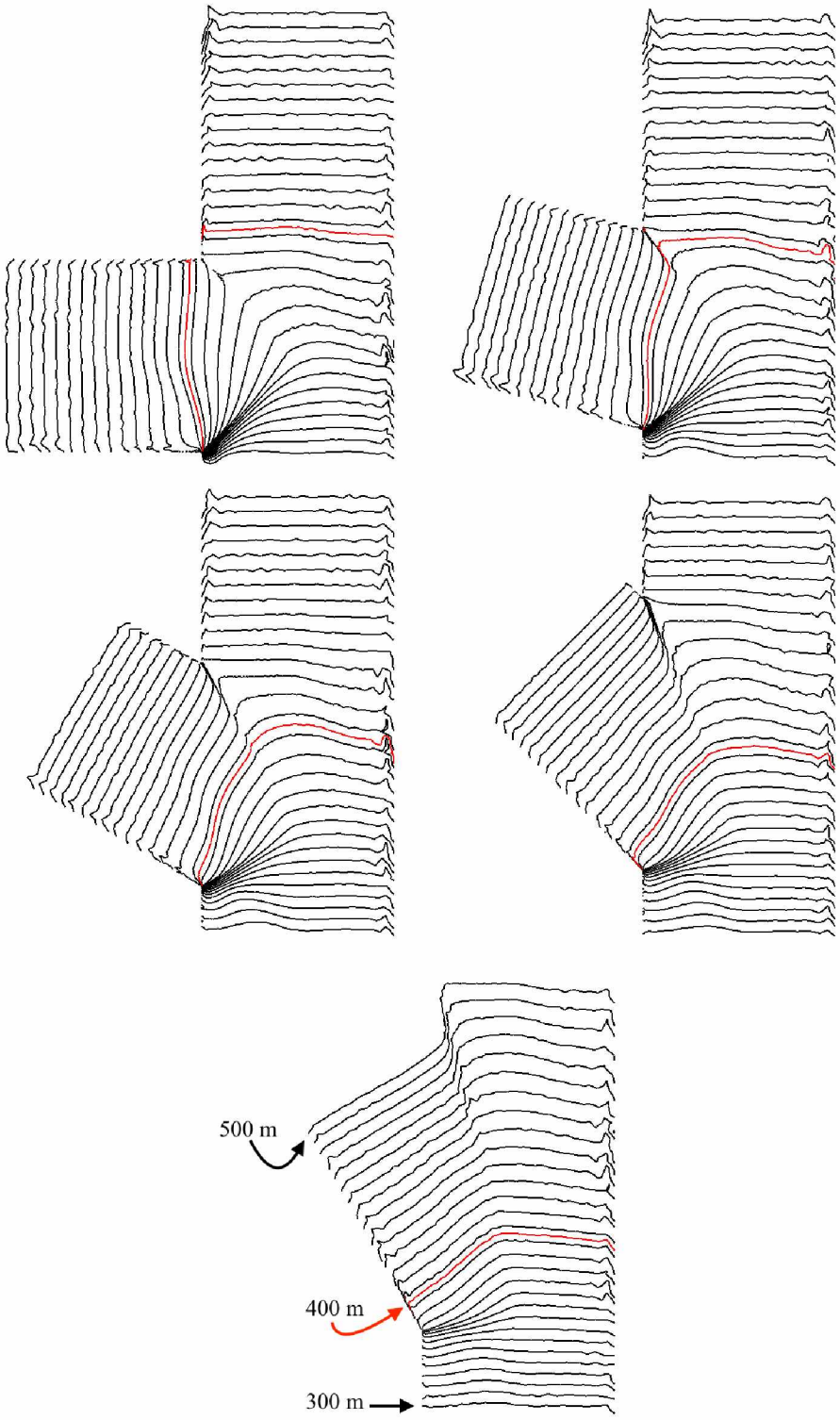


Figure 3.1. *Surface elevation contours at the confluence for θ values of 0°,15°,30°,45°,60° respectively. The red contour line signifies the 400 m contour. Contour lines have a 6.6 m spacing for surface elevations of 300 m to 500 m. The labels on the 60° surface elevation contours are constant throughout all contours shown.*

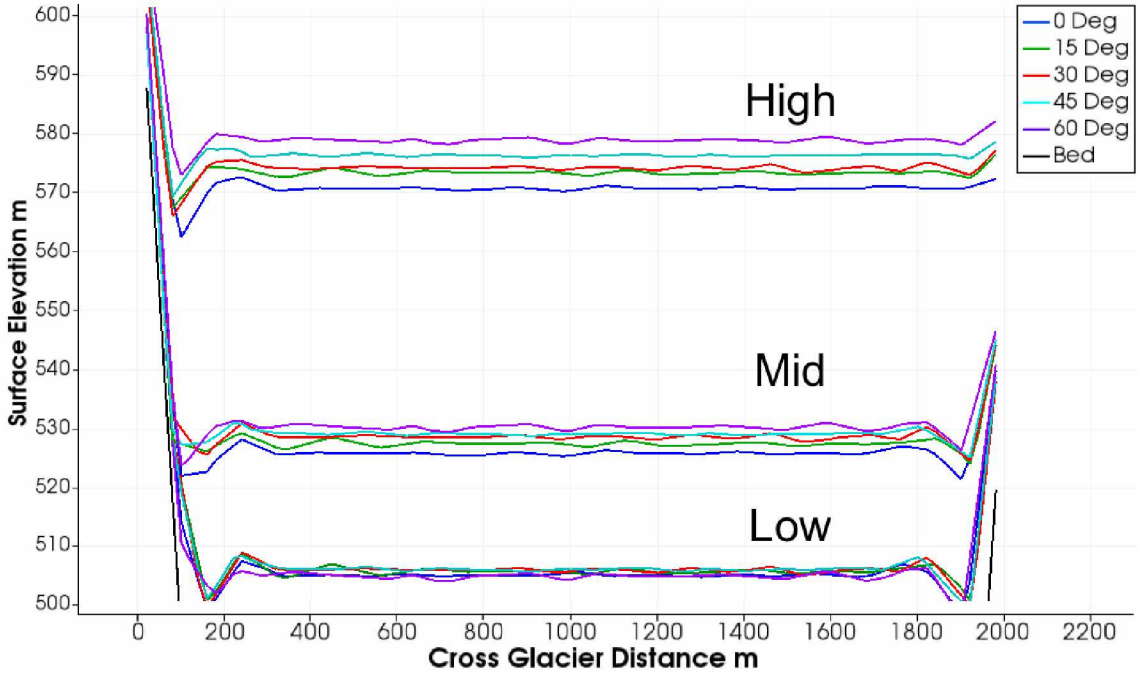


Figure 3.2. *Surface elevation at 5 km above the confluence zone with color cooresponding to tributary angle. Low refers to a relative flux of 0.77, Mid for 1.5, and High for 2.22.*

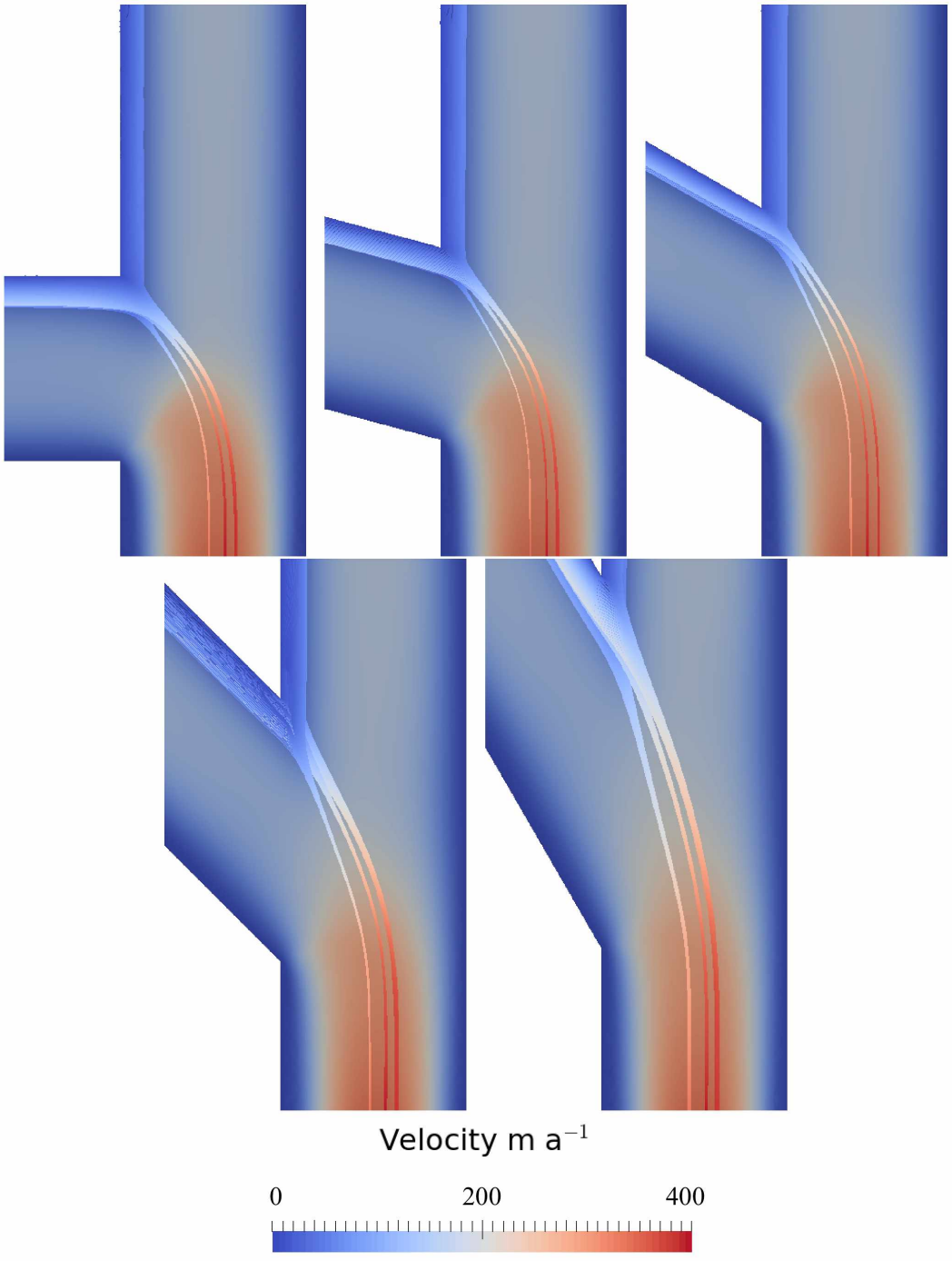


Figure 3.3. *The medial moraine location for each angle and for relative flux values of 0.77, 1.5, and 2.22.*

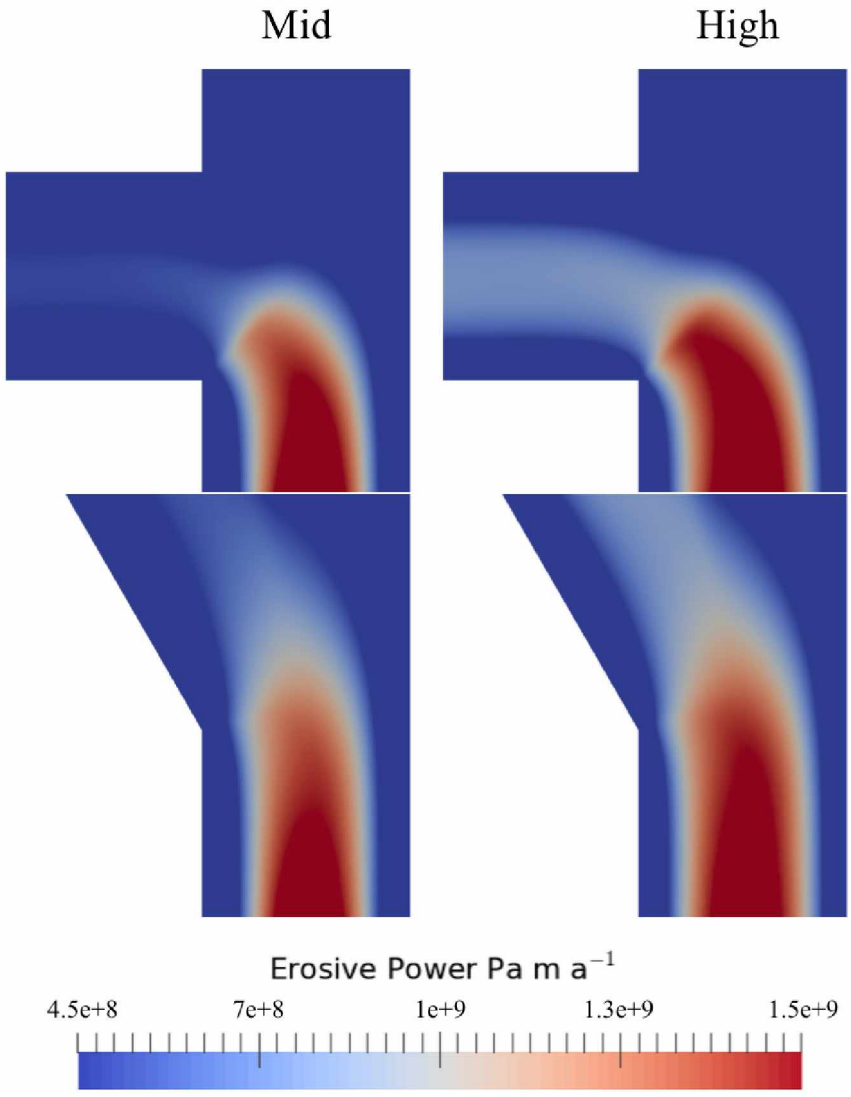


Figure 3.4. *Erosive power for the two extreme tributary angles at the Mid (1.5) and High (2.22) values of relative flux.*

# Chapter 4
# Discussion

## 4.1 Surface Elevation

There is a nonlinear relation between the relative flux and surface elevation (Fig. 4.1). The spread in surface values as the tributary angle increases could be caused by the different locations of the confluence junction. The elevation increases as the confluence's junction travels up-glacier as seen in Fig. (3.1). The measurement of the surface occurs 5 km up-glacier from the confluence center where the upper junction for $\theta = 0°$ is at 1 km and $\theta = 60°$ it is at 3.9 km from the confluence center. Fig. (3.2) and Fig. (4.1) show that the more important feature of a glacier to induce flow restrictions will be the tributary flux, with the tributary angle not having as strong an impact.

## 4.2 Erosive Power

When inspecting the confluence of two glacier branches, Gudmundsson and others (1997) show that a downward flow component at the medial moraine in the confluence area and an upward-flow component at the outer walls occur as a result of the confluence. Vertical velocities from these flow components would transport rocks and other debris to the glacier bed which could induce enhanced erosion of the glacier bed. MacGregor and others (2000) state that with a trunk/tributary junction a step or an overdeepening develops on the trunk valley floor immediately down-glacier of the confluence which agrees with our results of greatly increased erosive power in that region.

This would suggest that over time the glacier valley would evolve towards overdeepenings at the confluence. Such overdeepenings would better accommodate the fluxes from both branches and therefore presumably reduce the damming effect. If we assume a typical erosion rate of 1 mm $a^{-1}$ put forth by MacGregor and others (2000), it would take $10^5$ years to develop an overdeepening of 100m.

Glaciers in the Alaska Range that have surged such as Black Rapids Glacier are concentrated along the Denali Fault. The Denali Fault is a strike-slip fault under Black Rapids Glacier that has been observed to be slipping at a rate of 4.4 mm $a^{-1}$ with the southern portion closest to the Loket Tributary being displaced westward (up-glacier direction) (Haeussler and others, 2017). For a square kilometer of bed experiencing 1 mm $a^{-1}$ while

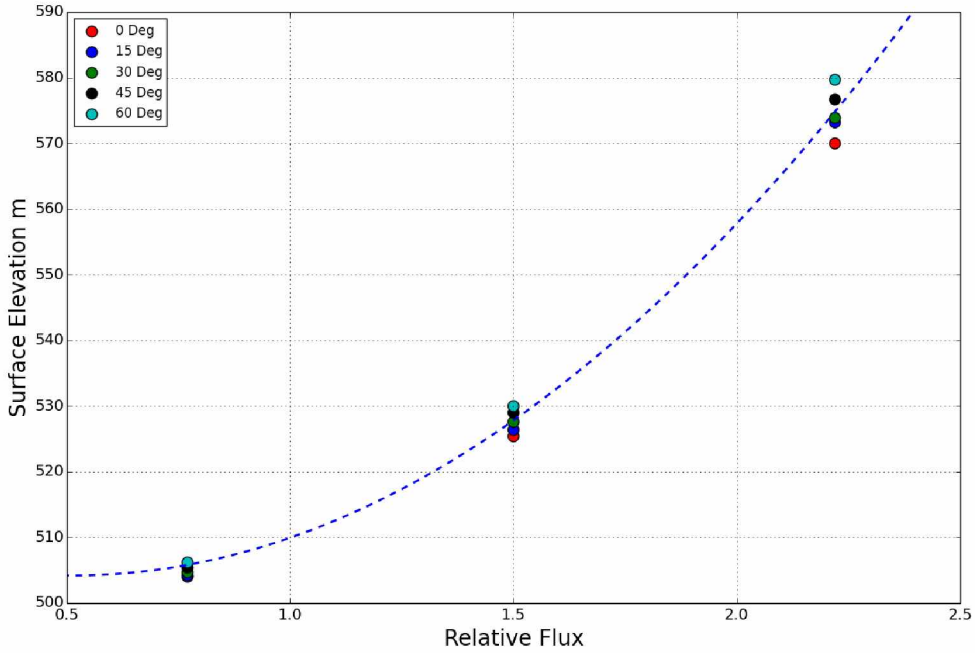


Figure 4.1. *Surface elevation with respect to relative flux. A parabolic fit illustrates the nonlinear relationship.*

slipping at 4.4 mm $a^{-1}$ the bed would erode down 125 m total in the time it would take that area of bed to move a kilometer out of the area of enhanced erosion. For a glacier on a strike-slip fault moving at 4.4 mm $a^{-1}$ the bed will only overdeepen by ~100 m at the confluence without including any feedback to erosion that may occur due to overdeepenings. Based on this, the movement of the Denali Fault could cause the eroding bed to move over time not allowing for overdeepenings to occur. This might enable a build-up to a surge geometry and therefore contribute towards the surge at Black Rapids Glacier.

### 4.3 Medial Moraine Location

The results of Fig. (3.3) show that altering the relative flux has a weakly nonlinear relationship for the position of the medial moraine which could arise from the parabolic geometry of the bed. From an observational standpoint measuring the medial moraine location into the trunk glacier can give an indication for the relative flux between the trunk and tribu-

tary. The location of the medial moraine also impacts where the abrasion from debris at the bed occurs. Gudmundsson and others (1997) believes that the medial moraine enhances erosion through this abrasion, but this transport was not considered in this work. The measured increase in velocity observed at the medial moraine can be associated with the no-slip condition from the friction of the valley sides no longer acting once in the confluence (Collins, 1970). Fig. (3.1) does not show a medial moraine surface feature, which would manifest as a small band of debris covered ice elevated above the neighboring ice where the two flows converge. Gudmundsson (1999) explains that debris cover that originated from the sides of the glacier valley follow these streamlines and reduce melt for the ice underneath causing differential ablation along the surface. The addition of an ablation term that depends on debris cover in our confluence would resolve this lack of a surface feature.

# Chapter 5
# Conclusion

This work was undertaken with the intent to glean insight into the response the trunk of a glacier has for varied tributary geometries and mass balance functions. We analyze the effects of tributary angle and relative flux on surface elevation, medial moraine location, and erosive power at the bed of the glacier. Tributary angle had a minimal effect on surface elevation and the area of enhanced erosion at the bed and no impact on medial moraine location after the confluence. The glacier's geometry showed increased sensitivity to changes in tributary flux in every case when compared to the response due to varied tributary angle. A change in surface elevation located 5 km up-glacier from the confluence with a spread of roughly 10 m could be obtained from changing tributary angle. The relative flux was able to alter the surface elevation at the same location by 75 m from an elevation with minimal tributary flux of 505 m to 580 m showing a 15% increase in ice thickness. Relative flux showed a strong nonlinear relationship for surface elevation and a weaker nonlinear relationship for medial moraine location.

This research was aimed at creating conditions similar to Black Rapids Glacier to inspect under what conditions critical geometries could be reached that would trigger an active surge, similar to what last occurred in 1936. The medial moraine from the Loket tributary is pushing out approximately 70% of the width of the main trunk which signifies a large relative flux between the two during quiescence which closely resembles the medial moraine location for our relative flux of 2.22. Realistically the bed would erode creating an overdeepening but in our model we choose to have a static bed. With this choice of bed we are simulating the effect of the Denali Fault motion moving Black Rapids Glacier's eroding bed out of the confluence to prevent overdeepenings. These results show the occurrence of a damming effect where there are higher surface elevations upstream of the confluence if there is more flux out of the tributary. Our results show that damming effects are possible with geometric settings resembling Black Rapids Glacier.

Future works that inspect effects of tributary geometry could include the following additions in conditions and geometries. Changing the channel's depth or entrance's cross sectional area in the tributary could lead to different scenarios such as the formation of icefalls. By mimicking friction loss due to basal water redistribution through altering

the basal drag term a surge event could be generated with the intent to observe surface adjustments during a surge event and the recovery after the event. Our mass balance function is constant in time and is used to define flux, but defining a mass balance function in terms of elevation is a far more realistic approach. As our flow restriction causes the elevation to rise up-glacier in the main trunk this would bring the ice into a cooler climate which would result in feedback effects. Accounting for the motion of the bed by imposing a displacement based on the motion of the Denali Fault and an erosion law could verify our hypothesis on why flow restrictions may have occurred at Black Rapids Glacier. Understanding the interplay between erosion and fault motion would help better define an erosive law for the situation of glaciers resting on strike-slip faults. These additions or alterations to what has been presented in this research would contribute to further improving the current understanding for surge initiation and the role tributaries play in the surge cycle.

## Bibliography


Ayachit U (2015) *The ParaView guide: a parallel visualization application*. Kitware, Inc., USA

Brinkerhoff D and Johnson J (2014) A stabilized finite element method for calculating balance velocities in ice sheets. *The Cryosphere*, **7**, 5183–5195

Brinkerhoff D and Johnson J (2015) Dynamics of thermally induced ice streams simulated with a higher-order flow model. **120**, 1743–1770

Clarke T (1991) Glacier dynamics in the Susitna River basin, Alaska, U.S.A. *Journal of Glaciology*, **37**(125), 97–106

Collins I (1970) A slip-line field analysis of the deformation at the confluence of two glacier streams. **9**, 169–193

Copland L, Sharp M and Dowdeswell J (2003) The distribution and flow characteristics of surge-type glaciers in the Canadian High Arctic. *Annals of Glaciology*, **36**, 73–81

Cuffey K and Paterson W (2010) *The physics of glaciers*. Elsevier, USA, 4 edition

Eisen O, Harrison W, Raymond C, Echelmeyer K, Bender G and Gorda J (2005) Variegated Glacier, Alaska, USA: a century of surges. *Journal of Glaciology*, **51**(174), 399–406

Geuzaine C and Remacle J (2009) Gmsh: A 3-D finite element mesh generator with built-in pre- and post-processing facilities. *International Journal for Numerical Methods in Engineering*, **79**(11), 1309–1331

Gudmundsson G (1999) A three-dimensional numerical model of the confluence area of Unteraargletscher, Bernese Alps, Switzerland. *Journal of Glaciology*, **45**, 219–230

Gudmundsson G, Iken A and Funk M (1997) Measurements of ice deformation at the confluence area of Unteraargletscher Bernese Alps, Switzerland. *Journal of Glaciology*, **43**(145), 548–556

Haeussler P, Matmon A, Schwartz D and Seitz G (2017) Neotectonics of interior Alaska and the late Quaternary slip rate along the Denali fault system. *Geosphere*, **13**(5), 1445–1463

Hamilton G and Dowdeswell J (1996) Controls on glacier surging in Svalbard. *Journal of Glaciology*, **42**(140), 157–168

Harrison W and Post A (2003) How much do we really know about glacier surging? *Annals of Glaciology*, **36**, 1–6

Heinrichs T, Mayo L, Echelmeyer K and Harrison W (1996) Quiescent-phase evolution of a surge-type glacier: Black Rapids Glacier, Alaska, U.S.A. *Journal of Glaciology*, **42**(140), 110–122

Herman F, Beyssac O, Brughelli M, Lane S, Leprince S, Adatte T, Lin J, Avouac J and Cox S (2015) Erosion by an alpine glacier. *Science*, **350**(6257), 193–195

Hewitt K (2007) Tributary glacier surges: an exceptional concentration at Panmah Glacier, Karakoram Himalaya. *Journal of Glaciology*, **53**(181), 181–188

Jiskoot H, Fox T and Van Wychen W (2017) Flow and structure in a dendritic glacier with bedrock steps. *Journal of Glaciology*, **63**(241), 912–928

Kamb B, Raymond C, Harrison W, Engelhardt H, Echelmeyer K, Humphrey N, Brugman M and Pfeffer T (1985) Glacier surge mechanism: 1982-1983 surge of Variegated glacier, Alaska. *Science (New York, N.Y.)*, **227**(4686), 469–479

Kargel J, Abrams M, Bishop M, Bush A, Hamilton G, Jiskoot H, Kääb A, Kieffer H, Lee E, Paul F, Rau F, Raup B, Shroder J, Soltesz D, Stainforth D, Stearns L and Wessels R (2005) Multispectral imaging contributions to global land ice measurements from space. *Remote Sensing of Environment*, **99**(1), 187 – 219

Kienholz C, Hock R, Truffer M, Bieniek P and Lader R (2017) Mass balance evolution of Black Rapids Glacier, Alaska, 1980–2100, and its implications for surge recurrence. *Frontiers in Earth Science*, **5**, 1–20

King O, Hambrey M, Irvine-Fynn T and Holt T (2015) The structural, geometric and volumetric changes of a polythermal Arctic glacier during a surge cycle: Comfortlessbreen, Svalbard. *Earth Surface Processes and Landforms*, **41**, 162–177

Logg A, Mardal K and Wells G (2012) *Automated solution of differential equations by the finite element method*. Springer, USA

MacGregor K, Anderson R, Anderson S and Waddington E (2000) Numerical simulations of glacial-valley longitudinal profile evolution. *Geology*, **28**(11), 1031–1034

Meier M and Post A (1969) What are glacier surges? *Canadian Journal of Earth Sciences*, **6**(4), 807–817

Murray T, Strozzi T, Luckman A, Jiskoot H and Christakos P (2003) Is there a single surge mechanism? Contrasts in dynamics between glacier surges in Svalbard and other regions. *Journal of Geophysical Research: Solid Earth*, **108**(B5), 1–15

Oerlemans J and van Pelt W (2015) A model study of Abrahamsenbreen, a surging glacier in northern Spitsbergen. *The Cryosphere*, **9**(2), 767–779

Pattyn F (2002) Transient glacier response with a higher-order numerical ice-flow model. *Journal of Glaciology*, **48**(162), 467–477

Pattyn F, Perichon L, Aschwanden A, Breuer B, de Smedt B, Gagliardini O, Gudmundsson G, Hindmarsh R, Hubbard A, V Johnson J, Kleiner T, Konovalov Y, Martin C, J Payne A, Pollard D, Price S, Rueckamp M, Saito F, Soucek O and Zwinger T (2008) Benchmark experiments for higher-order and full Stokes ice sheet models (ISMIP-HOM). *The Cryosphere*, **2**, 95–108

Raymond C (1987) How do glaciers surge? A review. *Journal of Geophysical Research: Solid Earth*, **92**(B9), 9121–9134

Satyabala S (2016) Spatiotemporal variations in surface velocity of the Gangotri Glacier, Garhwal Himalaya, India: study using synthetic aperture radar data. *Remote Sensing of Environment*, **181**, 151–161

Sevestre H and Benn D (2015) Climatic and geometric controls on the global distribution of surge-type glaciers: implications for a unifying model of surging. *Journal of Glaciology*, **61**(228), 646–662

Shugar D, Rabus B and Clague J (2010) Elevation changes (1949–1995) of Black Rapids Glacier, Alaska, derived from a multi-baseline InSAR DEM and historical maps. *Journal of Glaciology*, **56**(198), 625–634

Truffer M, Echelmeyer K and Harrison W (2001) Implications of till deformation on glacier dynamics. *Journal of Glaciology*, **47**(156), 123–134

Truffer M, Motyka R, Hekkers M, Howat I and King M (2009) Terminus dynamics at an advancing glacier: Taku Glacier, Alaska. *Journal of Glaciology*, **55**(194), 1052–1060